Structural and Computational Characterization of a Bridging Zwitterionic-Amidoxime Uranyl Complex

Journal:	*Organic Chemistry Frontiers*
Manuscript ID	QO-RES-02-2019-000267.R1
Article Type:	Research Article
Date Submitted by the Author:	06-Mar-2019
Complete List of Authors:	Decato, Daniel; University of Montana, Chemistry Berryman, Orion; University of Montana, Chemistry and Biochemistry Department; University of Montana, Chemistry

COMMUNICATION

Structural and Computational Characterization of a Bridging Zwitterionic-Amidoxime Uranyl Complex

Received 00th January 20xx,
Accepted 00th January 20xx

DOI: 10.1039/x0xx00000x

Daniel A. Decato, Orion B. Berryman*

A bridging (μ_2) neutral zwitterionic amidoxime binding mode previously unobserved between amidoximes and uranyl is reported and compared to other uranyl amidoxime complexes. Density functional theory computations show the dinuclear complex exhibits a shallow potential energy surface allowing for facile inclusion of a nonbonding water molecule in the solid-state.

While existing uranium resources are sufficient for current, and near-future global energy demands, ensuring a long-term and inexpensive supply of uranium is of global interest. Methods for securing long-term nuclear fuel sources are diverse, and include surveying new terrestrial sources[1] and improving the nuclear fuel cycle recyclability.[2–4] Another approach focuses on harvesting the 4.5 billion tons of uranium contained in the world's oceans.[5] However, the low uranium concentration of 3.3 parts per billion[6] and the relatively high concentration of other elements,[7] make selective uranium sequestration challenging. Nevertheless, scientists have pursued oceanic uranium for more than six decades, with reports in the 1980s shifting research focus from inorganic adsorbents to organic amidoxime (AO) based materials.[8,9] Since then, various AO uranyl extractants have been examined including nanoparticles,[10,11] ionic liquids,[12] carbon electrodes,[13] metal–organic frameworks,[14] covalent organic frameworks,[15] and hydrogels.[16] Yet AO functionalized polymers remain the most extensively studied and have led to considerable improvements in sorbent properties.[7,17] However, optimizing the selectivity of AO extractants for uranium over vanadium remains a challenge, likely exacerbated by the enigmatic binding modes to uranium. Identifying AO binding modes through structure elucidation of small molecule AO–uranyl complexes will continue to inform future designs of extractant technologies.

*Department of Chemistry and Biochemistry, University of Montana, 32 Campus Drive, Missoula, Montana, United States, 59812
Electronic Supplementary Information (ESI) available: ligand and complex synthetic schemes, gas-phase DFT calculations and coordinates, crystallographic refinement details, Cambridge Structural Database search details, CCDC 1897633. For ESI and crystallographic data in CIF or other electronic format seeDOI10.1039/x0xx00000x

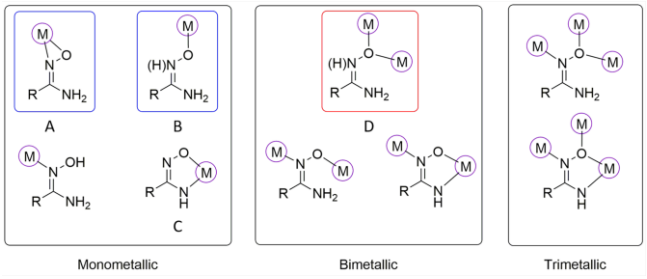

Figure 1. ChemDraw illustrations of known binding modes of amidoximes. Binding modes of previously reported AO–uranyl complexes are in blue boxes. The new AO–uranyl binding mode displayed in complex **1** is outlined with a red box.

AO ligands exhibit a variety of binding modes to metal ions (**Figure 1**).[18] In contrast, only two binding motifs have been experimentally demonstrated for small molecule AO–uranyl complexes, from a total of only seven structures in the Cambridge Structural Database (CSD) (**Figure S3**). In 1984 Witte et al. presented two AO–uranyl complexes; one with acetyl-amidoxime (AAO) and the other with phenyl-amidoxime (PhAO).[19] These seminal structures display zwitterionic AOs with an η^1-O binding through the oxime oxygen (**Figure 1B**). The remaining five structures exhibit side-on η^2-N,O binding through the N–O oxime bond (**Figure 1A**).[12,20–22] The η^2-N,O binding is the most stable in density functional theory (DFT) computations;[21] although, only by 0-3 kcal/mol, leading to a belief that the chelation (**Figure 1C**) and η^2-N,O binding modes may be in equilibrium in solution.[9,23] The presence of a chelate in AO polymeric fibers exposed to environmental seawater is supported by an extended X-ray absorption fine structure study. However, the authors acknowledged that an η^2-N,O binding mode could not be ruled out.[23] More recently, concentrated aqueous AAO solutions indicated three AOs complex uranyl via the η^2-N,O motif through computational and X-ray absorption spectroscopy studies.[24] The paucity of AO–uranyl complexes

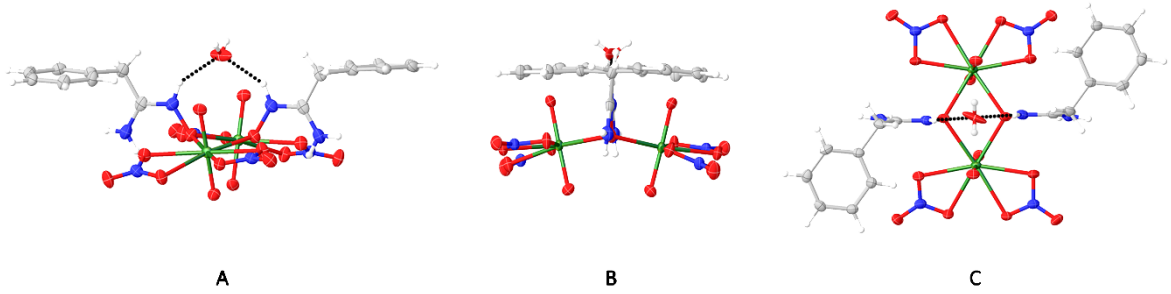

A B C

Figure 2 A) Hydrogen bonding interaction of **1** with the noncoordinating water B) Puckered conformation of **1**. C) **1** viewed down the crystallographic *b* axis. Hydrogen bonds are depicted as black dots. Thermal ellipsoids are drawn at the 50% probability level.

and inconclusive evidence of a dominate binding motif highlights the need for continued structural elucidation of AO–uranyl assemblies. Herein, we present a novel AO–uranyl binding mode, a bridging (μ_2) zwitterionic amidoxime, highlighted in the first dinuclear AO–uranyl complex.

Results and discussion

Crystals of $(UO_2)_2(NO_3)_4(\mu_2\text{-BnAO})_2{\bullet}H_2O$ (**1**) were formed by mixing $UO_2(NO_3)_2{\bullet}6H_2O$ and benzyl-amidoxime (BnAO) in a 1:1 molar ratio in nitromethane (**Scheme 1**). The solution was slowly evaporated, resulting in amorphous yellow crusts and yellow prisms suitable for single crystal X-ray diffraction studies (for further experimental details see ESI).

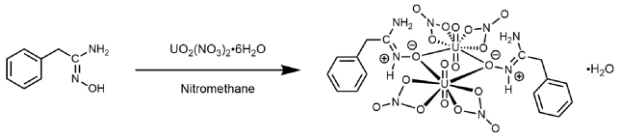

Scheme 1. ChemDraw illustrating the synthesis of **1**. Formal charges on the benzyl-amidoxime are shown to highlight tautomerization of the ligand. Nitrate ligands depicted with single bonds for clarity.

Structural description of (1)

The dinuclear uranyl complex (**1**) (**Figure 2**) crystallized in the monoclinic space group *C*2/*c*. The asymmetric unit displays one half of the complex (Z'=0.5) with the other half generated by a C_2 operation, resulting in identical coordination geometries for each uranium. Above the complex, residing on a two-fold axis, is a noncoordinating water molecule (**Figure 2C**). The uranium centers are 8-coordinate (6-coordinate equatorial) with distorted hexagonal bipyramidal geometry. Equatorial *cis*-bidentate nitrate anions are on the distal portion of the complex, while the remaining equatorial coordination sites are occupied by zwitterionic μ_2-BnAO ligands bridging the uranyl centers. The complex is puckered (**Figure 2B**), with uranyl oxygens tipped away from the tautomeric oxime nitrogen atoms, resembling a curvature evocative of uranyl–peroxide dimers and clusters.[25–29] Convergent and divergent uranyl oxygens are separated by 3.256(5) Å and 4.807(5) Å, respectively, while the uranium centers are 4.0513(3) Å apart. Unremarkably, the uranyl group is linear and symmetrical with $U–O_{oxo}$ bond lengths of 1.757(3) Å and 1.764(3) Å and a O=U=O angle of 178.83(12)° (**Table S1**).

Structural comparisons

The first reported AO–uranyl crystal structures display zwitterionic AOs binding to uranium in an η^1 fashion through the oxime oxygen.[19] These mononuclear 6-coordinate square bipyramidal uranium complexes exhibit four equatorial AOs and two charge balancing, noncoordinating nitrate anions. In contrast, the zwitterionic AO ligands of **1** are bridging, prompting structural comparisons to other AO–uranyl species (**Table S3**). The $U–O_{oxime}$ bond lengths are 2.442(2) Å and 2.466(2) Å for **1** while the reported averages for the η^1-AAO and η^1-PhAO tautomers are 2.307 Å and 2.26 Å respectively, indicating a weaker $U–O_{oxime}$ bond in **1**. The AO group of **1** has an $N–O_{oxime}$ bond length of 1.408(4) Å, $C–N_{oxime}$ bond length of 1.316(5) Å and $C–N_{amide}$ bond length of 1.310(5) Å. The similar lengths of $C–N_{oxime}$ and $C–N_{amide}$ in **1** suggest resonance stabilization of the positive charge by the lone pair of electrons on the N_{amide}. This is supported by slight $C–N_{amide}$ bond reduction of **1** when compared to other AO–uranyl structures (**Table S3**). Complex **1** demonstrates $C–N_{amide}$ bond shortening of ≈ 0.04 Å compared to the nonbridging η^1 zwitterionic structures reported. Similarly, the $C–N_{amide}$ bonds of η^2-AO–

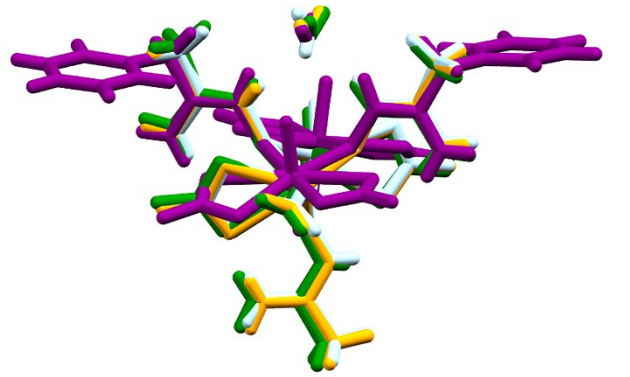

Figure 3 Structure overlay diagram of complex **1** and lanthanide structures with μ_2-zwitterionic AO ligands highlight their similarities. Additional noncoordinating waters, structure disorder and nitrate ligands have been omitted for clarity. Complex **1** is purple while the lanthanide structures reported by Kelly and Rodgers are green, orange, and light blue. Green– SEYXIG–Pr, Orange–SEYXUS–Nd, Blue–SEYXOM–Gd (Color in figure–CSD ref code–element symbol).

uranyl structures are longer than **1** by at least 0.03 Å. While organic AOs in the CSD display bond lengths similar to uranyl bound AOs (**Table S3**), the average C–N_{amide} bond lengths from this data set are longer than **1** by ≈ 0.04 Å. Surprisingly, the BnAO crystal structure is not reported in the CSD, however a *p*-bromine analogue has been reported (CSD ref code- GIKTIF).[30] The *p*-bromo-BnAO exhibits a C–N_{amide} bond length that is 1.359(2), almost 0.05 Å longer than in **1**. C–N_{oxime} and N–O_{oxime} bond lengths of the organic bromine derivative are 1.290(2) Å and 1.428(2) Å, respectively, trending with the organic AO averages (**Table S3**). Thus, upon complexation in a zwitterionic μ_2 fashion C–N_{amide} and N–O_{oxime} bonds decrease, while C–N_{oxime} bond increases which may have implications in metal-assisted reactions.[18,31] Similar to **1** a reduction of C–N_{amide} bond lengths has been observed in other bridging tautomeric AO structures donating hydrogen bonds to noncoordinating water molecules (*vide infra*). These structural observations suggest that the subtle contraction of the C–N_{amide} bond in **1** may be induced by the iminium hydrogen bonding to the noncoodinating water and/or the bridging motif.

Kelly and Rodgers recently reported homometallic dinuclear structures displaying zwitterionic μ_2-AAOs with neodymium, gadolinium, and praseodymium.[32] These lanthanide structures crystallized with noncoordinating water molecules and exhibit hydrogen bonding similar to **1** (**Figure 3**). In **1**, the water molecule accepts two symmetrical hydrogen bonds from the iminium nitrogen protons with donor-to-acceptor (N•••O) distances of 2.839(5) Å and N–H•••O angles of 143(4)°. The lanthanide complexes have three μ_2-AAOs resulting in combinations of iminium and amide hydrogen bonding. The bidentate iminium hydrogen bonding of these lanthanide complexes are longer than **1**, with N•••O distances ranging from 2.862–2.906 Å. with N–H•••O angles ranging from 140–174°. The hydrogen bond interaction between the iminium and the water in **1** may potentially stabilize the positive charge[32] while promoting the curvature of the complex.

Role of the noncoordinating water and crystal packing

The packing of**1** is largely dictated by hydrogen bonding (**Table S2**). Chains of complexes propagate along the crystallographic *c* axis due to hydrogen bonding of the AO amide. One hydrogen interacts with a nitrate oxygen with a donor-to-acceptor (N•••O) distance of 3.083(4) Å and a N–H•••O angle of 148(4)°, while the other hydrogen contacts the π-system of the phenyl ring (**Figure 4**). Neighboring chains are held together by the water hydrogen bonding to nitrate oxygens of flanking complexes with donor-to-acceptor (N•••O) distances of 3.112(3) Å and 3.000(3) Å with associated N–H•••O angles of 143(6)° and 149(6)°, respectively (**Figure S2**). This hydrogen bonding is vital to the packing, as there are no additional strong interactions holding adjacent complexes together. This contrasts with Rodgers' lanthanide complexes, where the water supports an existing hydrogen bond network between adjacent complexes. Thus, the inclusion of water in this solid-state structure of **1** is likely due to both favorable bidentate hydrogen bonding interactions with the complex as well as advantageous hydrogen bond network formation upon crystallization.

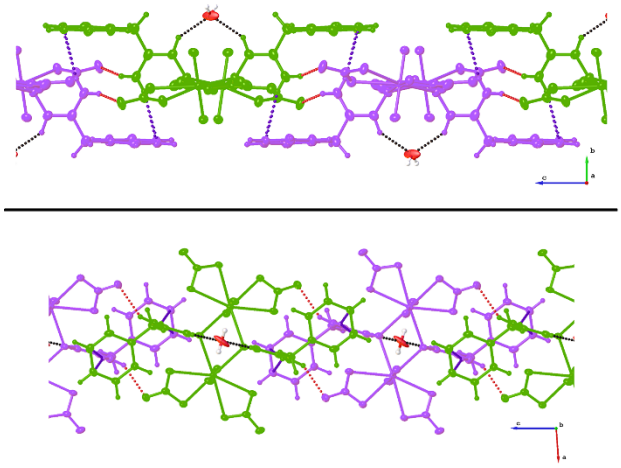

Figure 4 Intrachain hydrogen bonding of **1** as viewed down the crystallographic *a* (top) and *b* (bottom) axis. Adjacent complexes of **1** propagating in the *c* direction are represented in alternating colors of green and purple. Hydrogen bonds from the amide to the nitrate oxygens are depicted as red dotted lines, while N–H•••π contacts are illustrated by purple dotted lines to the nearest aryl carbon atoms. Iminium hydrogen bonds to the noncoordinating water are depicted by black dotted lines. Thermal ellipsoids are drawn at the 50% probability level.

Computations

The distinct curvature of **1** and the considerable hydrogen bonding network inspired us to examine the energy landscape of dinuclear μ_2-AO–uranyl complexes through DFT methods. The computations were performed using Gaussian09[33] at the B3LYP[34,35] level of theory. The Stuttgart RSC 1997 effective core potential was used for uranium,[36] while 6-31+G(d,p) basis sets were used for carbon, nitrogen, oxygen, and hydrogen atoms. The Stuttgart RSC 1997 effective core potential basis set was downloaded from the EMSL Basis Set Exchange.[37] The most diffuse function on uranium (having an exponent of 0.005) was removed from the basis to improve SCF convergence, a technique previously reported.[21] The combination of the B3LYP functional with the outlined basis sets has demonstrated accurate geometries and energetics for uranyl complexes.[38–45] Frequency calculations were performed to confirm that geometries were at a local minima. The computations were conducted using AAO ligands in place of BnAO ligands for simplicity.

Initially, we explored the potential energy surface through a rigid dihedral energy scan using the coordinates from the crystal structure of **1**. We varied the U···μ_2O···μ_2O···U dihedral to evaluate the energy required for the complex to pucker, as this distortion enables the water molecule to reside above the middle of the complex. The scan shows an unsymmetrical and shallow potential energy surface, where a 50° range of dihedral values fall within 10 kcal/mol of each other (**Figure 5** and **Table S5**). Unfavorable steric interactions between oxo-oxygens of the uranyl and oxime nitrogen atoms cause asymmetry. This

dihedral analysis highlights the ease of the complex to distort and accommodate a water molecule, enabling the hydrogen bonding network found in **1**. The potential energy surface resembles that of uranyl peroxide dimers, although the peroxide species are considerably more flexible.[25] To gain further insight into the energy landscape of dinuclear μ_2-AO–uranyl complexes, single point energy computations were evaluated for two different confirmations (**Figure 6**).

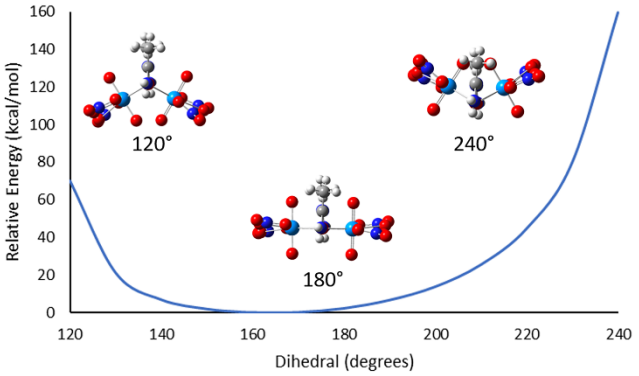

Figure 5 Computed relative energies of the AAO derivative of **1** as a function of dihedral angle.

A minimized structure of the AAO analogue of **1** without water (**AAO-1**) (**Figure 6A**) demonstrates a few distinct structural characteristics when compared to the solid-state structure of **1**. The absence of the water, results in a less puckered complex with a U···μ_2O···μ_2O···U dihedral of 174.57° (vs. 156.72(15)° for **1**). However, **AAO-1** twists and can be quantified by the O=U···U=O dihedral angle (See ESI for further details). This dihedral in the crystal structure of **1** is 9.75(18)° whereas the **AAO-1** is 42.38°. This distortion in **AAO-1** also results in hydrogen bonding between the AO ligands and the uranyl oxygens. hydrogen bonding to the uranyl oxygens has frequently been of interest[46–52] although hydrogen bonding to the uranyl oxygens are generally accepted as weak hydrogen bond acceptors. To further evaluate the role of the noncoordinating water, a minimization of an AAO analogue of **1** with a water molecule (**AAO-H_2O-1**) was carried out (**Figure 6B**). **AAO-H_2O-1** exhibits a U···μ_2O···μ_2O···U dihedral of 155.48°, and an O=U···U=O dihedral angle of 12.14° which are both comparable to **1**. The water in **AAO-H_2O-1** accepts two hydrogen bonds from the iminium hydrogens however the water rotates to donate a hydrogen bond to a uranyl oxygen. The energies of **AAO-H_2O-1** and **AAO-1** are similar (**AAO-1** is favored) with a difference of less than 5.2 kcal/mol. This further highlights the importance of the water in the solid-state packing and further demonstrates the low energy differences of these dinuclear complexes. The poor oxo acceptors and poor hydrogen bonding angles of the **AAO-1** also support the ability of a water to settle in the middle of the complex.

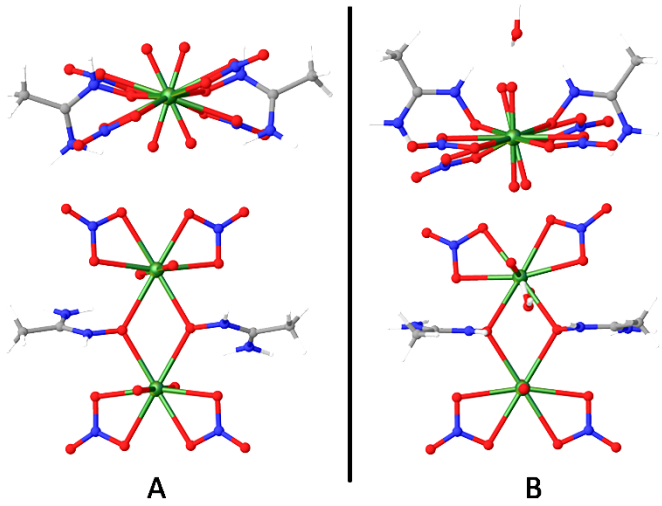

Figure 6 AAO analogues of **1**. A) Minimized structure **AAO-1** B) Minimized structure of **AAO-H_2O-1**

Previous computational evaluations of AO–uranyl complexes have largely focused on mononuclear structures with binding modes in **Figure 1A-C**. In contrast, evaluations of zwitterionic AO species are limited to a few computational papers evaluating AO tautomerization on uranium[53] and vanadium[54,55] binding as well as energetics of AO tautomerization.[56,57] Together these studies suggest AO tautomerization, before or after complexation, influences the binding mode and selectivity of AO based materials. Complex **1** validates the need to continue studying zwitterionic AOs for the pursuit of understanding AO uranophile selectivity. Furthermore, evaluations of multinuclear complexes through physical and theoretical methods would be a natural progression considering the large quantity of nonuranyl ions in natural settings.

Conclusions

We have presented a novel AO binding mode to the uranyl dication. Neutral zwitterionic μ_2-amidoxime ligands are present in the first example of a multinuclear AO-uranyl complex. The solid-state structure is highlighted by an extensive hydrogen bonding network constructed by the dinuclear complex and the noncoordinating water molecule. A DFT examination of the puckered complex illustrates the shallow potential energy surface that accommodates the water and is comparable to previously examined uranyl peroxide dimers. The computational investigations further highlight the importance of the noncoordinating water to facilitate the crystal packing observed. The paucity of AO-uranyl structural data underscores the importance of this work. These results provide another possibility for AO coordination which may be occurring in polymeric materials. The unique structure and binding are highlighted as a small piece of the puzzle in understanding AO–uranyl selectivity.

Acknowledgements

X-ray crystallographic data were collected at the University of Montana X-ray diffraction core facility supported by the Center for Biomolecular Structure and Dynamics CoBRE (National

Institutes of Health, CoBRE NIGMS P20GM103546). Single crystal X-ray diffraction data were collected using a Bruker D8 Venture, principally supported by NSF MRI CHE-1337908.

Conflicts of interest

"There are no conflicts to declare".

Notes and references

1 Nuclear Energy Agency and International Atomic Energy, *Uranium 2018*, OECD, 2019.
2 E. M. Wylie, K. M. Peruski, S. E. Prizio, A. N. A. Bridges, T. S. Rudisill, D. T. Hobbs, W. A. Phillip and P. C. Burns, *J. Nucl. Mater.*, 2016, **473**, 125–130.
3 S. Widder, *J. Renew. Sustain. Energy*, 2010, **2**, 062801.
4 E. A. Andrianova, V. D. Davidenko, V. F. Tsibulskiy and S. V. Tsibulskiy, *Phys. At. Nucl.*, 2015, **78**, 1252–1258.
5 R. V Davies, J. Kennedy, R. W. Mcilroy, R. Spence and K. M. Hill, *Nature*, 1964, **203**, 1110–1115.
6 K. Saito and T. Miyauchi, *J. Nucl. Sci. Technol.*, 1982, **19**, 145–150.
7 J. Kim, C. Tsouris, R. T. Mayes, Y. Oyola, T. Saito, C. J. Janke, S. Dai, E. Schneider and D. Sachde, *Sep. Sci. Technol.*, 2013, **48**, 367–387.
8 B. F. Parker, Z. Zhang, L. Rao and J. Arnold, *Dalt. Trans.*, 2018, **47**, 639–644.
9 C. W. Abney, R. T. Mayes, T. Saito and S. Dai, *Chem. Rev.*, 2017, **117**, 13935–14013.
10 L. Huang, L. Zhang and D. Hua, *J. Radioanal. Nucl. Chem.*, 2015, **305**, 445–453.
11 D. Li, S. Egodawatte, D. I. Kaplan, S. C. Larsen, S. M. Serkiz, J. C. Seaman, K. G. Scheckel, J. Lin and Y. Pan, *Environ. Sci. Technol.*, 2017, **51**, 14330–14341.
12 P. S. Barber, S. P. Kelley and R. D. Rogers, *RSC Adv.*, 2012, **2**, 8526.
13 C. Liu, P.-C. Hsu, J. Xie, J. Zhao, T. Wu, H. Wang, W. Liu, J. Zhang, S. Chu and Y. Cui, *Nat. Energy*, 2017, **2**, 17007.
14 L. Chen, Z. Bai, L. Zhu, L. Zhang, Y. Cai, Y. Li, W. Liu, Y. Wang, L. Chen, J. Diwu, J. Wang, Z. Chai and S. Wang, *ACS Appl. Mater. Interfaces*, 2017, **9**, 32446–32451.
15 C. Bai, M. Zhang, B. Li, X. Zhao, S. Zhang, L. Wang, Y. Li, J. Zhang, L. Ma and S. Li, *RSC Adv.*, 2016, **6**, 39150–39158.
16 F. Wang, H. Li, Q. Liu, Z. Li, R. Li, H. Zhang, L. Liu, G. A. Emelchenko and J. Wang, *Sci. Rep.*, 2016, **6**, 19367.
17 L. Rao, *Recent International R&D Activities in the Extraction of Uranium from Seawater*, Berkeley, CA (United States), 2010.
18 D. S. Bolotin, N. A. Bokach and V. Y. Kukushkin, *Coord. Chem. Rev.*, 2016, **313**, 62–93.
19 E. G. Witte, K. S. Schwochau, G. Henkel and B. Krebs, *Inorganica Chim. Acta*, 1984, **94**, 323–331.
20 S. P. Kelley, P. S. Barber, P. H. K. Mullins and R. D. Rogers, *Chem. Commun.*, 2014, **50**, 12504–12507.
21 S. Vukovic, L. A. Watson, S. O. Kang, R. Custelcean and B. P. Hay, *Inorg. Chem.*, 2012, **51**, 3855–3859.
22 Q. Sun, B. Aguila, J. Perman, A. S. Ivanov, V. S. Bryantsev, L. D. Earl, C. W. Abney, L. Wojtas and S. Ma, *Nat. Commun.*, 2018, **9**, 1644.
23 C. W. Abney, R. T. Mayes, M. Piechowicz, Z. Lin, V. S. Bryantsev, G. M. Veith, S. Dai and W. Lin, *Energy Environ. Sci.*, 2016, **9**, 448–453.
24 L. Zhang, M. Qie, J. Su, S. Zhang, J. Zhou, J. Li, Y. Wang, S. Yang, S. Wang, J. Li, G. Wu and J. Q. Wang, *J. Synchrotron Radiat.*, 2018, **25**, 514–522.
25 P. D. Dau, P. V. Dau, L. Rao, A. Kovács and J. K. Gibson, *Inorg. Chem.*, 2017, **56**, 4186–4196.
26 P. Miró, S. Pierrefixe, M. Gicquel, A. Gil and C. Bo, *J. Am. Chem. Soc.*, 2010, **132**, 17787–17794.
27 B. Masci and P. Thuéry, *Polyhedron*, 2005, **24**, 229–237.
28 J. Qiu, B. Vlaisavljevich, L. Jouffret, K.

Nguyen, J. E. S. Szymanowski, L. Gagliardi and P. C. Burns, *Inorg. Chem.*, 2015, **54**, 4445–4455.

29 B. Vlaisavljevich, L. Gagliardi and P. C. Burns, *J. Am. Chem. Soc.*, 2010, **132**, 14503–14508.

30 C. B. Aakeröy, A. S. Sinha, K. N. Epa, P. D. Chopade, M. M. Smith and J. Desper, *Cryst. Growth Des.*, 2013, **13**, 2687–2695.

31 V. Y. Kukushkin, D. Tudela and A. J. L. Pombeiro, *Coord. Chem. Rev.*, 1996, **156**, 333–362.

32 S. P. Kelley and R. D. Rogers, *Supramol. Chem.*, 2018, **30**, 411–417.

33 M. J. Frisch, G. W. Trucks, H. B. Schlegel, G. E. Scuseria, M. A. Robb, J. R. Cheeseman, G. Scalmani, V. Barone, B. Mennucci, G. A. Petersson, H. Nakatsuji, M. Caricato, X. Li, H. P. Hratchian, A. F. Izmaylov, J. Bloino, G. Zheng, J. L. Sonnenberg, M. Hada, M. Ehara, K. Toyota, R. Fukuda, J. Hasegawa, M. Ishida, T. Nakajima, Y. Honda, O. Kitao, H. Nakai, T. Vreven, J. A. J. Montgomery, J. E. Peralta, F. Ogliaro, M. Bearpark, J. J. Heyd, E. Brothers, K. N. Kudin, V. N. Staroverov, R. Kobayashi, J. Normand, K. Raghavachari, A. Rendell, J. C. Burant, S. S. Iyengar, J. Tomasi, M. Cossi, N. Rega, N. J. Millam, M. Klene, J. E. Knox, J. B. Cross, V. Bakken, C. Adamo, J. Jaramillo, R. Gomperts, R. E. Stratmann, O. Yazyev, A. J. Austin, R. Cammi, C. Pomelli, J. W. Ochterski, R. L. Martin, K. Morokuma, V. G. Zakrzewski, G. A. Voth, P. Salvador, J. J. Dannenberg, S. Dapprich, A. D. Daniels, O. Farkas, J. B. Foresman, J. V. Ortiz, J. Cioslowski and D. J. Fox, 2009.

34 A. D. Becke, *J. Chem. Phys.*, 1993, **98**, 5648–5652.

35 C. Lee, W. Yang and R. G. Parr, *Phys. Rev. B*, 1988, **37**, 785–789.

36 M. Dolg, H. Stoll, H. Preuss and R. M. Pitzer, *J. Phys. Chem.*, 1993, **97**, 5852–5859.

37 K. L. Schuchardt, B. T. Didier, T. Elsethagen, L. Sun, V. Gurumoorthi, J. Chase, J. Li and T. L. Windus, *J. Chem. Inf. Model.*, 2007, **47**, 1045–1052.

38 G. A. Shamov, G. Schreckenbach, R. L. Martin and P. J. Hay, *Inorg. Chem.*, 2008, **47**, 1465–1475.

39 G. Schreckenbach, P. J. Hay and R. L. Martin, *J. Comput. Chem.*, 1999, **20**, 70–90.

40 K. E. Gutowski, V. A. Cocalia, S. T. Griffin, N. J. Bridges, D. A. Dixon and R. D. Rogers, *J. Am. Chem. Soc.*, 2007, **129**, 526–536.

41 M. Bühl and G. Schreckenbach, *Inorg. Chem.*, 2010, **49**, 3821–3827.

42 J. L. Sonnenberg, P. J. Hay, R. L. Martin and B. E. Bursten, *Inorg. Chem.*, 2005, **44**, 2255–2262.

43 G. Schreckenbach, P. J. Hay and R. L. Martin, *Inorg. Chem.*, 1998, **37**, 4442–4451.

44 L. P. Spencer, P. Yang, B. L. Scott, E. R. Batista and J. M. Boncella, *Inorg. Chem.*, 2009, **48**, 2693–2700.

45 M. Bühl, N. Sieffert, A. Chaumont and G. Wipff, *Inorg. Chem.*, 2011, **50**, 299–308.

46 L. A. Watson and B. P. Hay, *Inorg. Chem.*, 2011, **50**, 2599–2605.

47 T. S. Franczyk, K. R. Czerwinski and K. N. Raymond, *J. Am. Chem. Soc.*, 1992, **114**, 8138–8146.

48 P. H. Walton and K. N. Raymond, *Inorganica Chim. Acta*, 1995, **240**, 593–601.

49 S. Kannan, M. Kumar, B. Sadhu, M. Jaccob and M. Sundararajan, *Dalt. Trans.*, 2017, **46**, 16939–16946.

50 A. C. Sather, O. B. Berryman and J. Rebek, *Chem. Sci.*, 2013, **4**, 3601.

51 A. C. Sather, O. B. Berryman and J. Rebek, *J. Am. Chem. Soc.*, 2010, **132**, 13572–13574.

52 J. A. Platts and R. J. Baker, *Phys. Chem. Chem. Phys.*, 2018, **20**, 15380–15388.

53 C. Yang, S. Pei, B. Chen, L. Ye, H. Yu and S. Hu, *Dalt. Trans.*, 2016, **45**, 3120–3129.

54 N. Mehio, A. S. Ivanov, A. P. Ladshaw, S. Dai and V. S. Bryantsev, *Ind. Eng. Chem. Res.*, 2016, **55**, 4231–4240.

55 N. Mehio, J. C. Johnson, S. Dai and V. S. Bryantsev, *Phys. Chem. Chem. Phys.*, 2015, **17**, 31715–31726.

56 A. S. Novikov and D. S. Bolotin, *J. Phys. Org. Chem.*, 2018, **31**, e3772.

57 H. Tavakol and S. Arshadi, *J. Mol. Model.*,

2009, **15**, 807–816.